Supporting Information

Achieving High Performance Ultra-Broadband Near-infrared Emission through Multi Lattice Sites Occupancy and Energy Transfer for NIR LED Applications

*Mingkai Wei [a], Zixi Chen [a], Yongying Chen [a], Xinxiang Liang [a], Na Li [a], Xuejie Zhang [a, *], Wei Li [a], Haoran Zhang [a], Maxim S. Molokeev [b], and Bingfu Lei [a, *]*

[a] Key Laboratory for Biobased Materials and Energy of Ministry of Education, College of Materials and Energy, South China Agricultural University Guangzhou 510642, Guangdong, P. R. China
[b] Department of Physics and Technical Sciences, Western Caspian University, Baku, AZ 1001, Azerbaijan

Corresponding authors E-mail: **tleibf@scau.edu.cn (Bingfu Lei),** zhangxuejie@scau.edu.cn

Supplementary formula

The crystal field parameters for the crystal field of Cr^{3+} ions in an octahedral environment are calculated as follows:[1]

$$10D_q = E(4A_2 \rightarrow 4T_1) (1)$$

$$\frac{D_q}{B} = \frac{15(m-8)}{m^2-10m} \ (2)$$

$$m = \frac{E(4A_2-4T_1)-E(4A_2-4T_2)}{D_q} (3)$$

The internal quantum efficiency (IQE) is defined as the percentage of emitted photons relative to the number of absorbed photons. This is calculated using the following equation:

$$IQE = \frac{\int L_s}{\int E_R - \int E_s} \times 100\% \ (4)$$

where, L_S represents the number of photons emitted from the sample, E_R denotes the number of exciting photons, and E_S signifies the number of reflected photons for the $BaSO_4$ reference. The external quantum efficiency (EQE) is defined as the percentage of emitted photons relative to the number of excitation photons. This is calculated using the following equation:

$$EQE = \frac{\int L_s}{\int E_R} \times 100\% \ (5)$$

The absorption efficiency (AE) is defined as the percentage of the number of absorbed photons (by the sample) to that of excitation photons:

$$AE = \frac{\int E_R - \int E_s}{\int E_R} \times 100\% \ (6)$$

So the EQE is also calculated using the following equation:

$$EQE = IQE \times AE \times 100\% \ (7)$$

Supplementary figures and tables

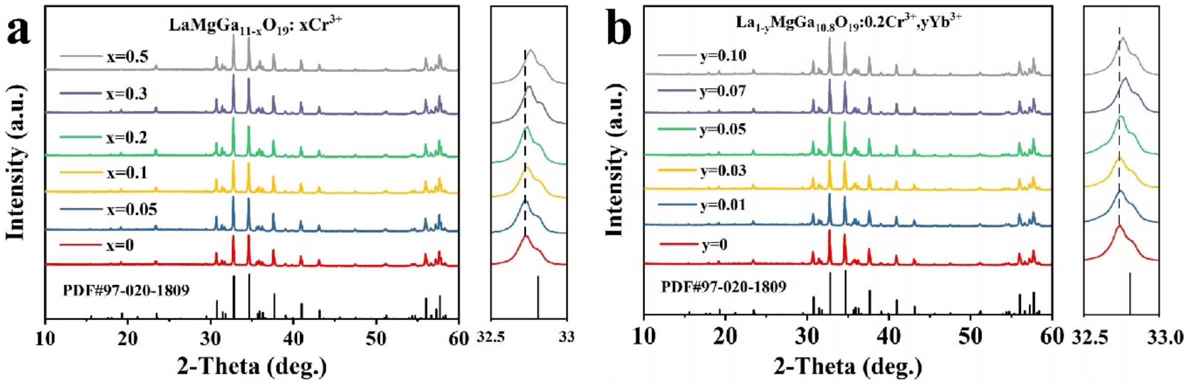

Figure S1 XRD patterns of (a) LMG:xCr^{3+} & (b) LMG:0.2Cr^{3+} ,yYb^{3+}.

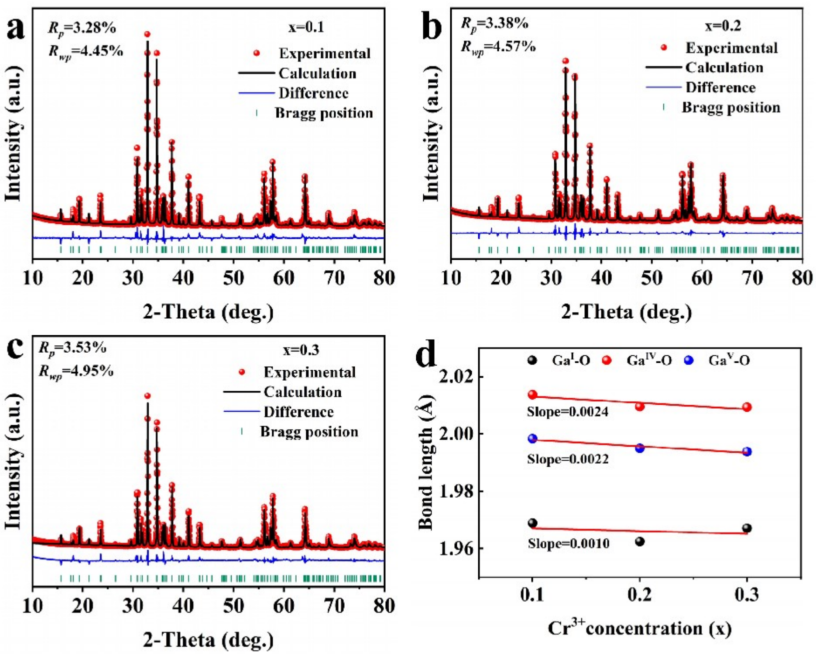

Figure S2 Rietveld refinement of (a) LMG:0.1Cr^{3+} & (b) LMG:0.2Cr^{3+}& (c) LMG:0.3Cr^{3+}. (d) Variation of Ga-O bond length with doping concentration of Cr^{3+} ions.

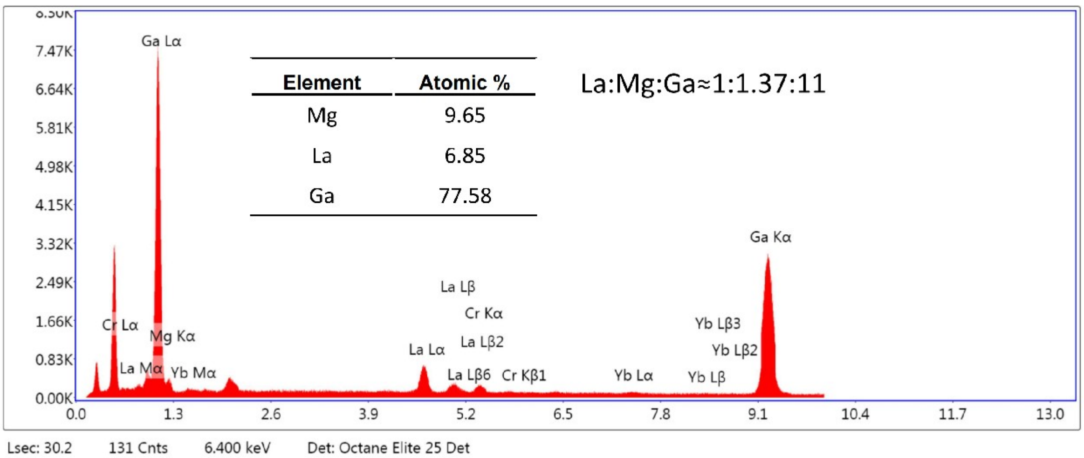

Figure S3 Elemental mappings (La, Mg,Ga, Cr and Yb).

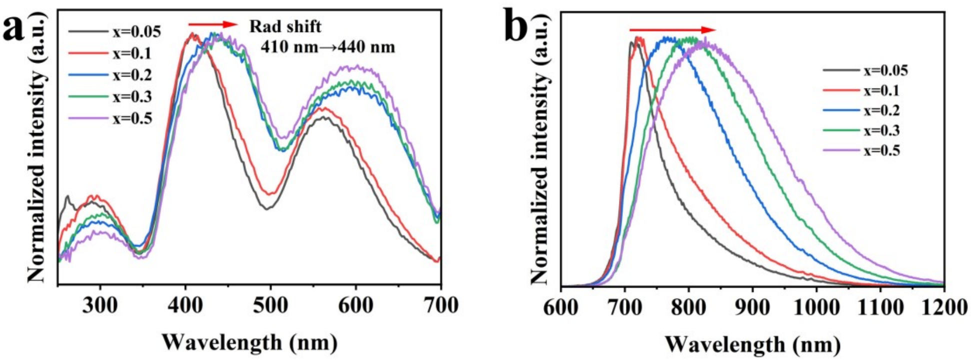

Figure S4 (a) excitation and (b) emission spectra of LMG:xCr^{3+}(x=0.05-0.5).

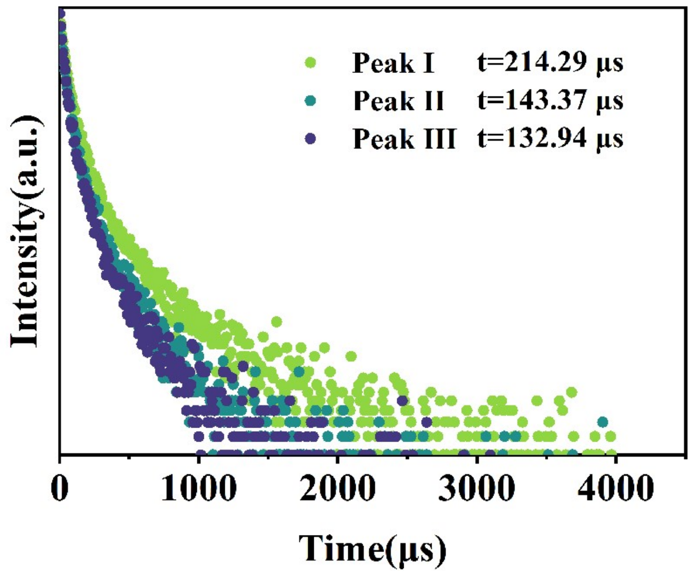

Figure S5 Fluorescence decay curves at three peaks.

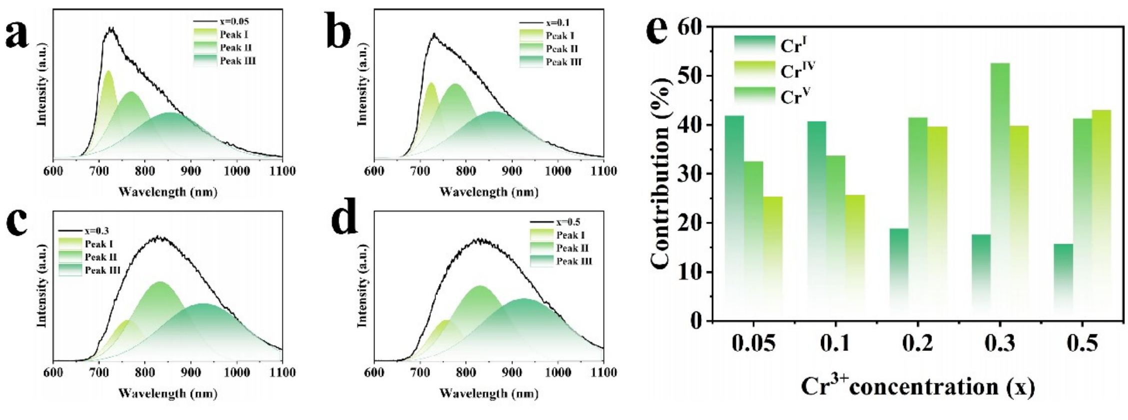

Figure S6 Peak-differentiating and imitating of (a) LMG:$0.05Cr^{3+}$ and (b) LMG:$0.1Cr^{3+}$ and (c) LMG:$0.3Cr^{3+}$ and (d) LMG:$0.5Cr^{3+}$. (e) Variation curves of the three peaks of LMG: xCr^{3+}(x=0.05-0.5).

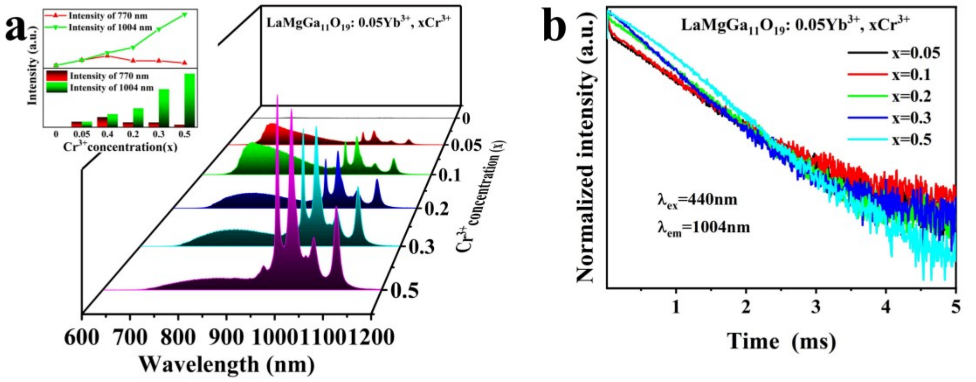

Figure S7 (a) Emission spectra of LMG:0.05Yb^{3+}, xCr^{3+}. (b) Fluorescence decay curves of LMG:0.05Yb^{3+}, xCr^{3+}.

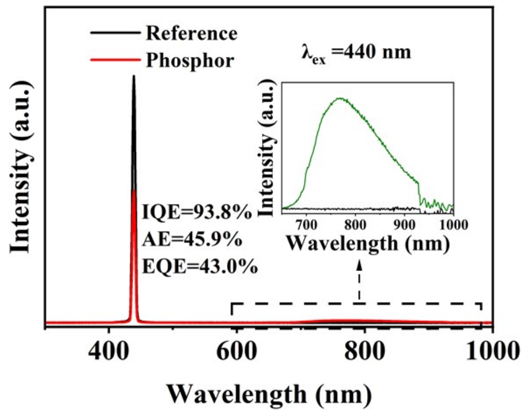

Figure S8 IQE, AE and EQE of LMG:0.2Cr^{3+}.

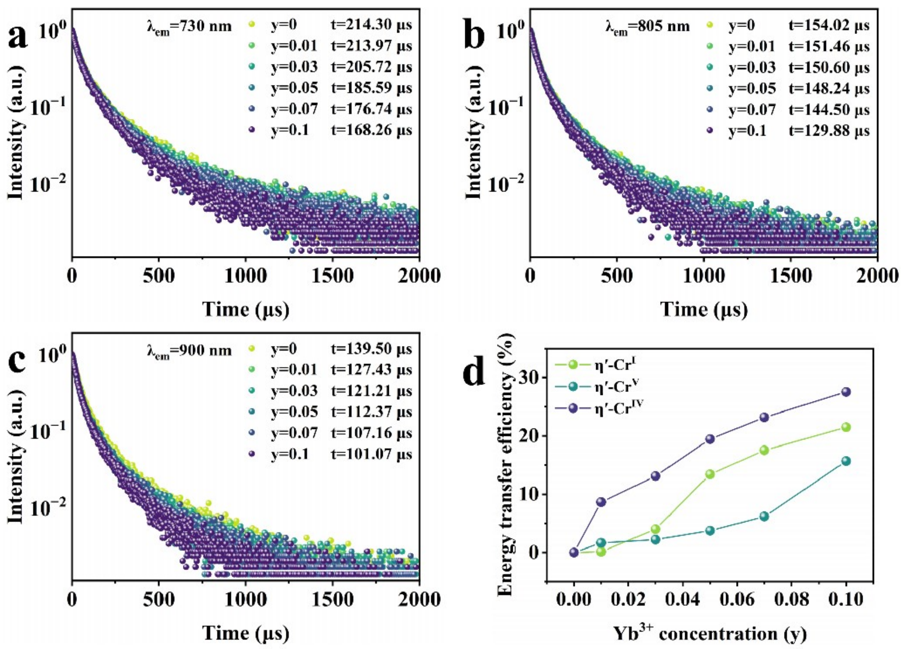

Figure S9 Fluorescence lifetimes at (a) 730 nm, (b) 805 nm and (c) 900 nm versus Yb^{3+} ion doping concentration. (d) Energy transfer efficiency versus Yb^{3+} concentration calculated from fluorescence lifetime data.

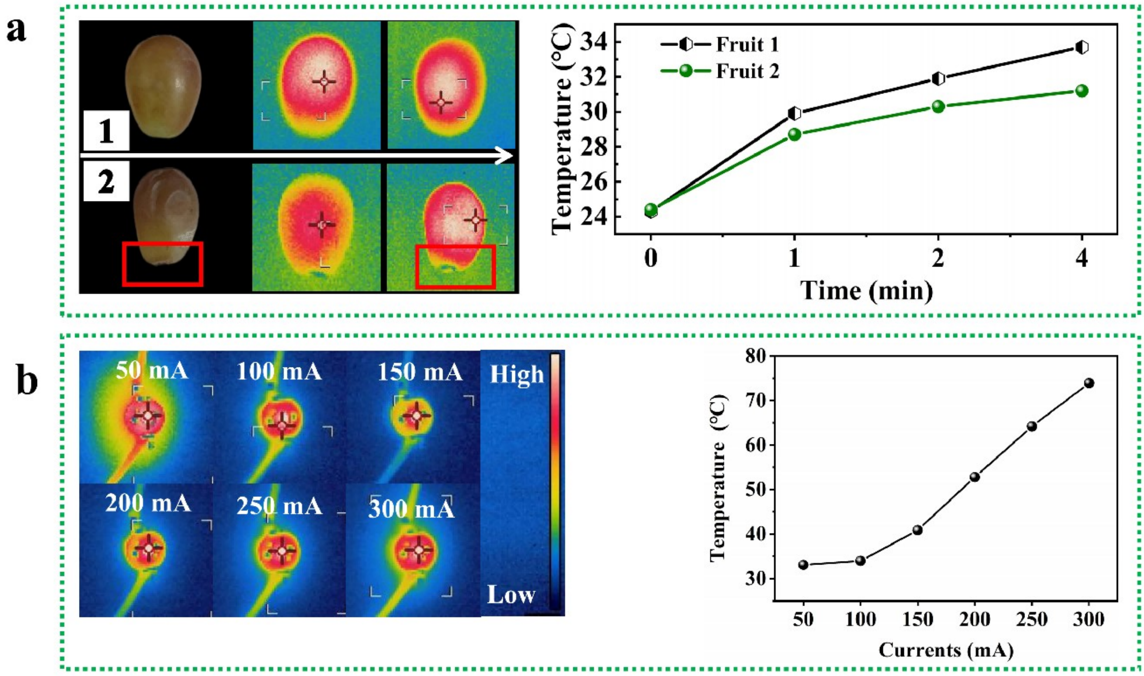

Figure S10 (a) Relationship between the temperature of fruit and the duration of NIR pc-LED exposure. (b) Relationship between operating temperature and operating current of NIR prototype devices.

Table S1 Main parameters of processing and refinement of the LMG:0.2Cr^{3+},0.05Yb^{3+} sample.

Formula	$LaMgGa_{11}O_{19}$:0.2Cr^{3+},0.05Yb^{3+}
Sp. Gr.	$P6_3/mmc$
a (Å)	5.794620(14)
c (Å)	22.67195(27)
V (Å^3)	659.279(24)
Z	2
2ϑ-interval, º	10-80
R_{wp}, %	3.09
R_p, %	1.79
χ^2	2.08

Table S2 Fractional atomic coordinates of $LaMgGa_{11}O_{19}$:0.2Cr^{3+},0.05Yb^{3+}.

Atom	x	y	z
La1	2/3	-2/3	1/4
La2	0.73286(14)	-0.73286(14)	1/4
Yb1	2/3	-2/3	1/4
Ga1	0	0	0
Mg1	0	0	0
Cr1	0	0	0
Ga2	0	0	0.23982(36)
Ga3	1/3	-1/3	0.027(27)
Mg2	1/3	-1/3	0.03(12)
Ga4	1/3	-1/3	0.189651(98)
Cr4	1/3	-1/3	0.189651(98)
Ga5	-0.16607(21)	0.16607(21)	0.10835(53)
Cr5	-0.16607(21)	0.16607(21)	0.10835(53)
O1	0	0	0.15235(48)
O2	2/3	-2/3	0.06122(47)
O3	0.18925(11)	-0.18925(11)	1/4
O4	0.14962(88)	-0.14962(88)	0.05560(24)
O5	0.50945(86)	-0.50945(86)	0.15248(29)

Table S3 Bond length data of Ga^1-O, Ga^4-O, and Ga^5-O octahedron.

Ga^1-O		Ga^4-O		Ga^5-O	
1.946 Å	Average 1.946 Å	1.991 Å	Average 1.983 Å	2.004 Å	Average 1.971 Å
1.946 Å		1.991 Å		2.004 Å	
1.946 Å		1.991 Å		1.990 Å	
1.946 Å		1.975 Å		1.905 Å	
1.946 Å		1.975 Å		1.905 Å	
1.946 Å		1.975 Å		2.023 Å	

Table S4. IQE, EQE, thermal stability and Photoelectric properties of Cr^{3+} and Yb^{3+} co-doped NIR emitting phosphor.

Phosphor	IQE (%)	EQE (%)	Thermal stability（%） @ temperture	NIR output power (mW) @ photoelectric efficiency	Ref.
$SrGa_4O_7$:Cr^{3+},Yb^{3+}	31.4	/	74%@423 K	11.1 mW@100 mA	[2]
Sr_2ScTaO_6:Cr^{3+},Yb^{3+}	/	/	78.4%@373 K	/	[3]
$Ca_2LuZr_2Al_3O_{12}$:Cr^{3+},Yb^{3+}	77.2	/	/	41.8 mW@100 mA	[4]
$(Ca_{0.5}Li_{0.5})(Mg_{0.5}Sc_{0.5})Si_2O_6$: Cr^{3+},Yb^{3+}	46	/	69%@423 K	~35.9 mW@100 mA	[5]
La_2MgHfO_6:Cr^{3+},Yb^{3+}	69	18.4	81.6%@373 K	/	[6]
$Mg_4Nb_2O_9$:Cr^{3+},Yb^{3+}	72.6	36	63%@373 K	~38.5 mW@100 mA	[7]
$LaMgGa_{11}O_{19}$:Cr^{3+},Yb^{3+}	94.2	40.8	89.3%@373 K 72.7%@423 K	28.3 mW@100 mA	This work

Table S5 Detailed measured data of the NIR pc-LED output power and efficiency under different current drive.

Current（mA）	Voltage（V）	Input electrical power (mW)	NIR output power (mW)	photoelectric efficiency (%)
20	2.65	53	6.0	11.3
50	2.74	137	14.1	10.3
100	2.85	285	28.3	9.9
150	2.84	426	41.5	9.7
200	2.91	582	53.4	9.2
250	2.96	742	64.9	8.7
350	3.08	1080	84.5	7.8

Reference

1 F. Zhu, Y. Gao, C. Zhao, J. Pi and J. Qiu, *ACS Appl. Mater. Interfaces*, 2023, **15**, 39550–39558.

2 Y. Xu, L. Luo, W. Zhao, W. Zhang and Z. Hu, *Optical Materials*, 2023, **145**, 114460.

3 Z. Shao, X. Zhou, L. Li, Y. Wang, F. Ling, C. Jing, X. Tang and Z. Cao, *Ceramics International*, 2023, **49**, 32860–32867.

4 S. He, L. Zhang, H. Wu, H. Wu, G. Pan, Z. Hao, X. Zhang, L. Zhang, H. Zhang and J. Zhang, *Advanced Optical Materials*, 2020, **8**, 1901684.

5 T.-Y. Hwang, Y. Choi, Y. Song, N. S. A. Eom, S. Kim, H.-B. Cho, N. V. Myung and Y.-H. Choa, *J. Mater. Chem. C*, 2018, **6**, 972–979.

6 H. Suo, Y. Wang, X. Zhao, X. Zhang, L. Li, K. Guan, W. Ding, P. Li, Z. Wang and F. Wang, *Laser & Photonics Reviews*, 2022, **16**, 2200012.

7 M. Zheng, X. Dong, D. Wu, Y. Wang, W. Zhou, Y. Liu and L. Zhang, *AIP Advances*, 2024, **14**, 055133.

Article titles of bibliographic references

1 Achieving Broadband NIR-I to NIR-II Emission in an All-Inorganic Halide Double-Perovskite $Cs_2NaYCl_6:Cr^{3+}$ Phosphor for Night Vision Imaging

2 Highly efficient and stable near-infrared broadband luminescence in $SrGa_4O_7:Cr^{3+}$, Yb^{3+} phosphor

3 Broadband near-infrared double-perovskite phosphor $Sr_2ScTaO_6:Cr^{3+}$, Yb^{3+} for NIR pc-LED applications

4 Efficient Super Broadband NIR $Ca_2LuZr_2Al_3O_{12}:Cr^{3+},Yb^{3+}$ Garnet Phosphor for pc-LED Light Source toward NIR Spectroscopy Applications

5 A noble gas sensor platform: linear dense assemblies of single-walled carbon nanotubes (LACNTs) in a multi-layered ceramic/metal electrode system (MLES)

6 Rapid Nondestructive Detection Enabled by an Ultra-Broadband NIR pc-LED

7 Cr^{3+} and Yb^{3+} co-doped perovskite-like phosphor with improved thermal stability by efficient energy transfer